

Seventh Quarterly Progress Report
N01-DC-9-2107

**The Neurophysiological Effects of
Simulated Auditory Prosthesis
Stimulation**

H. Mino, J.T. Rubinstein, C.A. Miller, P.J. Abbas

Department of Otolaryngology - Head and Neck Surgery
Department of Speech Pathology and Audiology
Department of Physiology and Biophysics
Department of Biomedical Engineering
University of Iowa
Iowa City, IA 52242

July 31, 2001

Contents

1	Introduction	2
2	Summary of activities in this quarter	2
3	Effects of the electrode-to-fiber distance on neural responses	3
3.1	Introduction	3
3.2	Methods	3
3.3	Results	6
3.4	Discussion	13
4	Plans for the next quarter	13
5	Appendix: Presentations and publications	14
6	Appendix: Numerical calculations	14

1 Introduction

The purpose of this contract is to explore issues involving the transfer of information from implantable auditory prostheses to the central nervous system. Our investigation is being pursued along multiple tracks and include the use of animal experiments and computer model simulations to:

1. Characterize the fundamental spatial and temporal properties of intracochlear stimulation of the auditory nerve.
2. Evaluate the use of novel stimuli and electrode arrays.
3. Evaluate proposed enhancements in animal models of partial degeneration of the auditory nerve.

In this seventh quarterly progress report (QPR), we focus on the first of these three aims, reporting on computer simulations characterizing the temporal response properties of single auditory nerve fibers as the electrode-to-fiber distance varies.

2 Summary of activities in this quarter

In our seventh quarter (1 May - 31 July, 2001), the following activities related to this contract were completed:

1. Refinements in the thin film electrode array have been designed and implemented. Recordings have been made on additional experimental animals.
2. Assessment of temporal properties of adaptation over long-term pulse train presentations have been done using the compound action potential.
3. Several parameters of the biophysical model have been investigated to assess the effects on temporal response properties of the neuron. Some results of that work are presented in this quarterly progress report.
4. A manuscript has been accepted for publication in the IEEE Transactions on Biomedical Engineering for the October, 2001 issue entitled "Analysis of Monophasic and Biphasic Electrical Stimulation of Nerve" by Rubinstein, Miller, Mino & Abbas.

3 Effects of the electrode-to-fiber distance on neural responses

3.1 Introduction

Computer simulation studies have played an important role in investigating the influence of various parameters on nerve fiber excitation. For computer simulation of extracellular electrical stimulation, McNeal developed a multi-compartment cable model (McNeal, 1976), with nodes of Ranvier represented by the conventional deterministic non-linear dynamics (Hodgkin and Huxley, 1952; Frankenhauser and Huxley, 1964). For auditory nerve fibers, some modeling works using McNeal's cable model have been found (Colombo and Parkins, 1987; Finley et al., 1990). Likewise, since it is important for cochlear implants to consider fluctuation phenomena (Verveen, 1961; Rubinstein, 1995) in the temporal response of spikes (Finley et al., 1990), a cable model has been developed in which stochastic sodium channels are incorporated into nodes of Ranvier (Matsuoka et al., 2001). However, it is still unclear how the temporal variation of spikes due to sodium channel current fluctuations (e.g., latency and jitter observed in experiments (Miller et al., 1999)) can be influenced by the geometry of auditory nerve fiber and of stimulus electrode. In this seventh QPR, we investigate the effects of the electrode-to-fiber distance on the temporal response properties, especially for jitter, utilizing a revised nerve fiber model incorporated with the advanced computational algorithm for generating ion channel current fluctuations (Mino et al, 2000; 2001).

3.2 Methods

Auditory nerve fibers were represented by a multi-compartment cable model with 50 nodal sections in which the parameters were set at: diameters D of $2.5 \mu m$, axon diameters d of $1.5 \mu m$, internodal lengths L of $230 \mu m$, and nodal gap width l of $1 \mu m$, as shown in Figure 1. One section between nodes in the axon model consisted of 10 compartments: the 1 nodal compartment expressing stochastic non-linear active nodes and the 9 internodal components expressing deterministic passive myelin sheath with internodal resistances r_m ($209 \times 140 M\Omega mm$), internodal capacitances ($1.6/30 pF/mm$), and axoplasmic resistances r_a (axoplasmic resistivity $1063 \times 6 \Omega mm$). The resistances and capacitances were modified from those parameters summarized in (Matsuoka et al., 2001) so as to generate plausible neural responses.

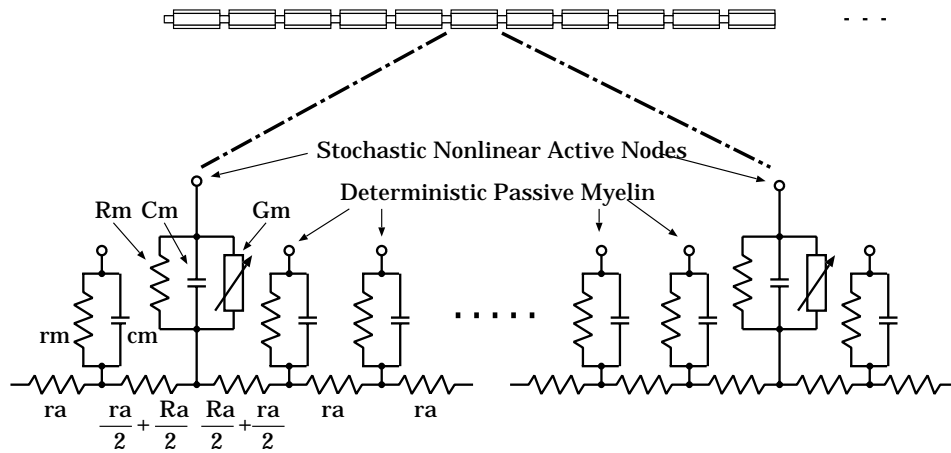


Figure 1: An auditory nerve fiber modeled by the multi-compartment cable model with stochastic non-linear active nodes and deterministic passive myelin sheath. One section between nodes in the axon model were represented by 10 compartments, 1 nodal and 9 internodal components.

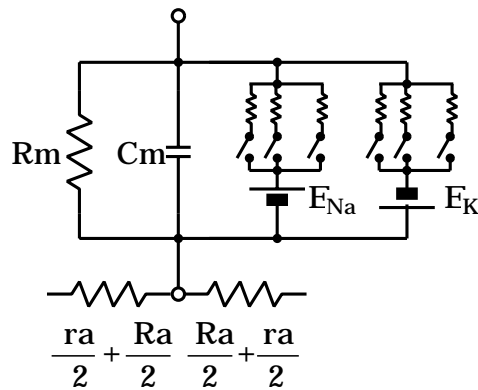


Figure 2: Stochastic non-linear active nodes modeled by the 130 sodium channels, the 50 potassium channels, and the voltage-independent nodal resistance and capacitance.

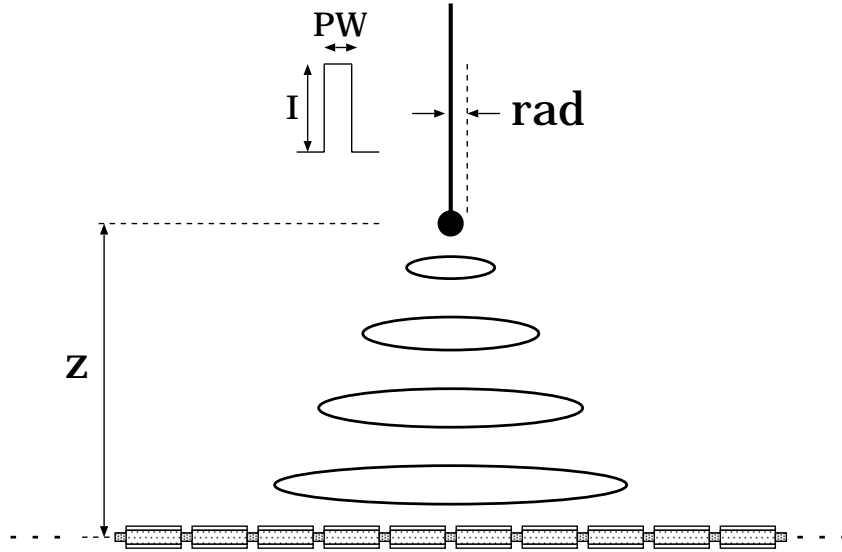


Figure 3: The geometry of electrode and axon. The electrode was located at distances z of 1, 4, and 7 mm above the center node (26th) of the simulated axon. Monophasic cathodic current pulses were presented in which the pulse width (PW) was set at 40 μs . The current pulse is supposed to create a variation in electric fields between the electrode and the axon, as indicated by rings.

The 50 nodes of Ranvier were represented by the 130 sodium channels with conductances γ_{Na} of 22.65 pS , the 50 potassium channels with conductances γ_K of 50.0 pS , the voltage-independent nodal resistance R_m (831 $M\Omega mm^2$), the nodal capacitance C_m (0.041 $\mu F/mm^2$), the nodal axoplasmic resistance R_a (axoplasmic resistivity $1063 \times 6 \Omega mm$), as shown in Figure 2. The resting potential and the reversal potentials for sodium and potassium channels were respectively set at -78 mV , 66 mV , and -88 mV . Each stochastic ion channel was assumed to be open or closed independently according to a Markov jumping process with voltage-dependent transition rates, and implemented by the advanced computational algorithm on the basis of the channel number tracking algorithm (Mino et al., 2000).

An electrode with radius of 1 μm was assumed to lie in a purely resistive homogeneous isotropic conducting bone (extracellular resistivity, $\rho_e = 25000 \Omega mm$), and was located at distances z of 1, 4, and 7 mm above the center node (26th) of the simulated axon, as shown in Figure 3. Monophasic cathodic current pulses with a duration of 40 μs were presented as stimuli.

The transmembrane potentials were generated by solving a diffusive partial differential equation with the Crank-Nicholson method (See Appendix), which was calculated on the basis of the average of explicit forward and implicit backward Euler integrations (Press et al., 1993). The transmembrane potentials of 1 *ms* in time length were generated for each simulation in which sampling steps were set at 5 μ s.

3.3 Results

Figure 4 shows the transmembrane potentials recorded at the 36th node, $V_m(36, t)$, in response to 50 identical stimulus pulses at the electrode-to-fiber distances of 1 *mm* in (a), 4 *mm* in (b), and 7 *mm* in (c), where the stimulus electrode was located above the 26th node. The transmembrane potential is relative to the resting potential.

Figure 5 shows the post stimulus time (PST) histogram generated from spike times of $V_m(36, t)$'s in response to 500 identical stimulus pulses at the electrode-to-fiber distances of 1 *mm* in (a), 4 *mm* in (b), and 7 *mm* in (c). The estimated firing efficiency(FE), jitter(JT), and conduction velocity(CV) are shown in each inset. The conduction velocity was estimated by averaging time differences between spike times at the 36th and 46th nodes. The jitter increased as the electrode-to-fiber distance increased. The values of jitter at distances of 7 *mm* are comparable to those observed in experiments using cat's single auditory fibers (Miller et al., 1999).

A large jitter at larger distances is likely due to two factors: (i) "spatial influence", the spatial distribution of the nodes initiated by stimuli tends to be wider as the electrode-to-fiber distance increases; (ii) "temporal influence", the temporal variations at each node tend to be larger as the electrode-to-fiber distance increases. The temporal variations may be generated by activating a small number of stochastic sodium channels under subthreshold situations.

Figure 6 depicts the histogram of spike initiations at each node at the electrode-to-fiber distances of 1 *mm* in (a), 4 *mm* in (b), and 7 *mm* in (c). The 500 stimulus current pulses were presented for each histogram at which FE was approximately 0.5, so that the number of samples was approximately 250 in each histogram. The spatial distribution tends to be wider as the electrode-to-fiber distance increases, as expected intuitively.

Figure 7 shows the PST histogram of the nodal initiation sites at the electrode-to-fiber of 1 *mm*. The spike times were recorded at the 36th node

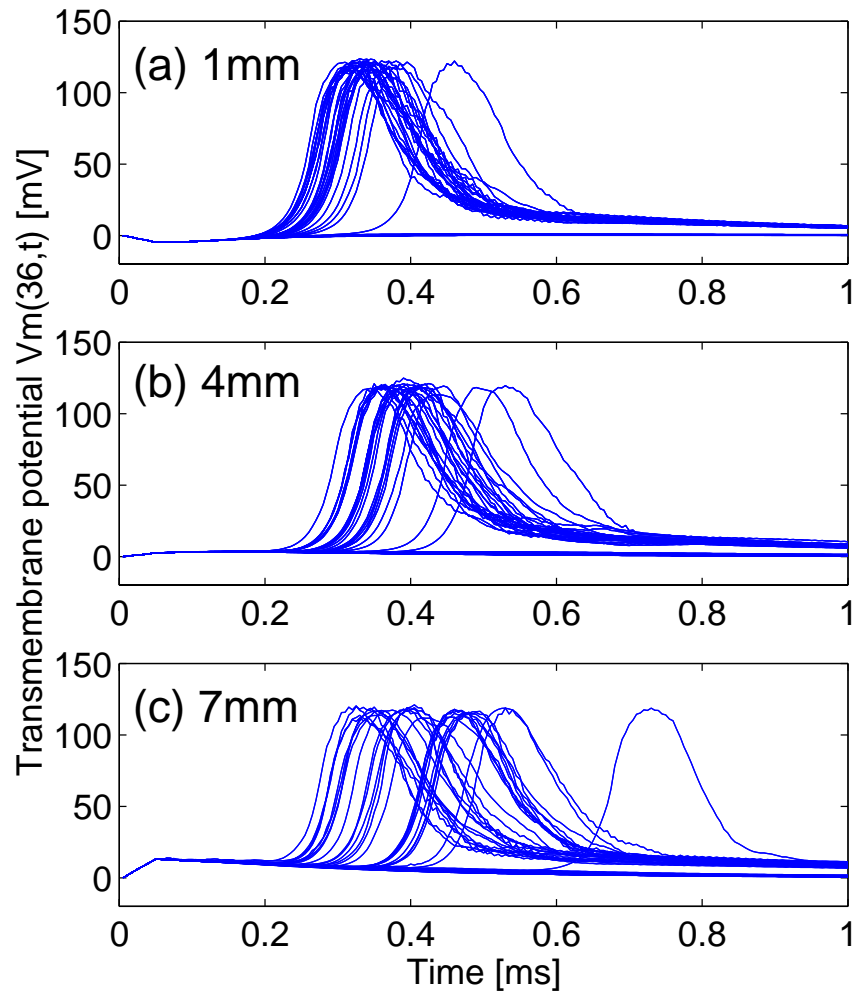


Figure 4: Transmembrane potentials recorded at the 36th node, $V_m(36,t)$, in response to 50 identical stimulus pulses at the electrode-to-fiber distances of 1 mm in (a), 4 mm in (b), and 7 mm in (c). Transmembrane potential is relative to the resting potential.

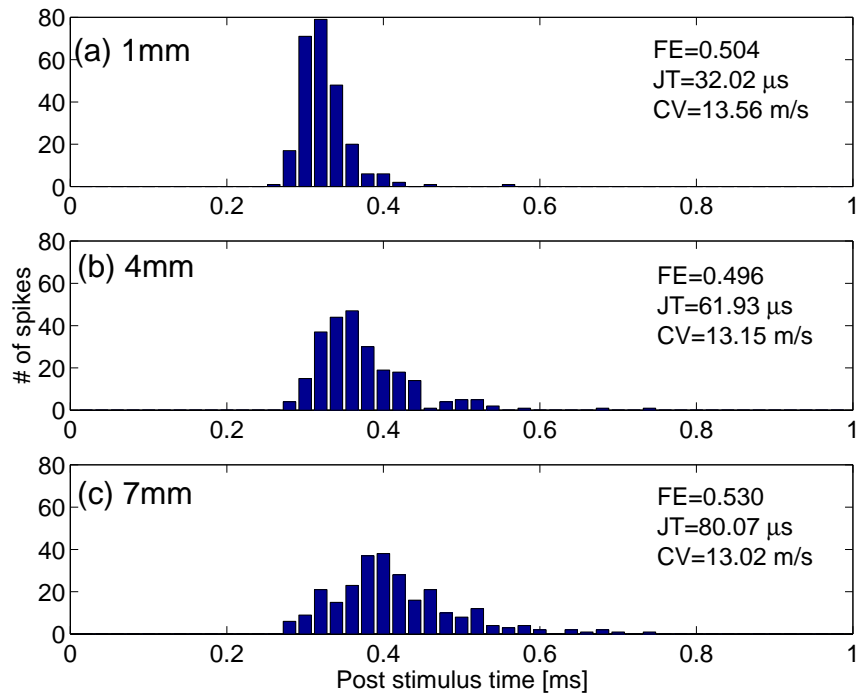


Figure 5: The PST histogram generated from the spike times of $V_m(36, t)$'s in response to 500 identical stimulus pulses at the electrode-to-fiber distances of 1 mm in (a), 4 mm in (b), and 7 mm in (c). The estimated firing efficiency (FE), jitter (JT), and conduction velocity (CV) are shown in each inset.

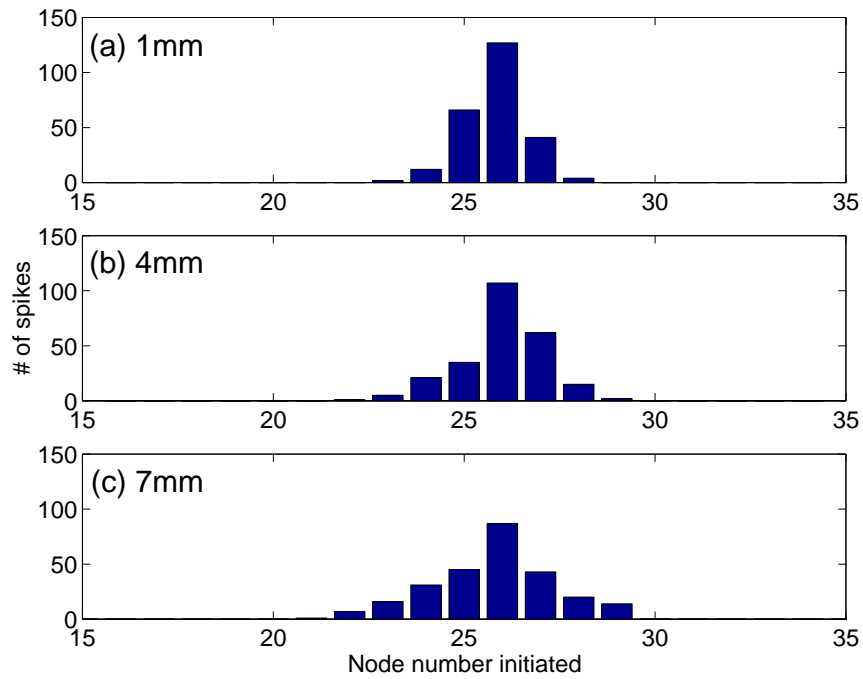


Figure 6: The histogram of spike initiations at each node at the electrode-to-fiber distances of 1 mm in (a), 4 mm in (b), and 7 mm in (c). The 500 stimulus current pulses were presented. The number of spike occurrences was counted by measuring $V_m(36, t)$ at the 36th node.

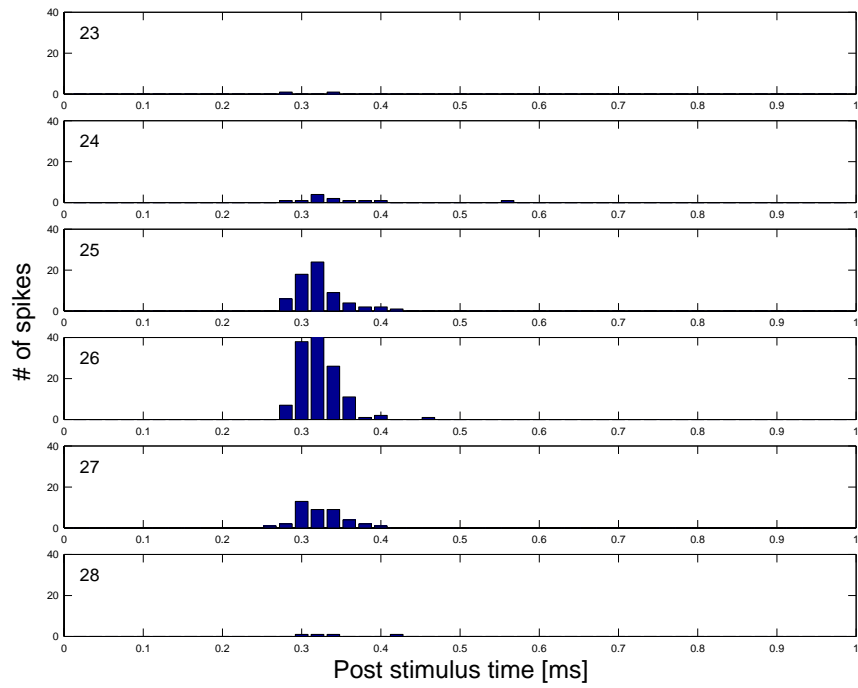


Figure 7: The PST histogram of each nodal initiation site at the electrode-to-fiber distance of 1 *mm*. The PST histogram was generated from the spike times of $V_m(36, t)$'s in response to 500 identical stimulus pulses in which the spikes were initiated at the nodes from the 23th to the 28th.

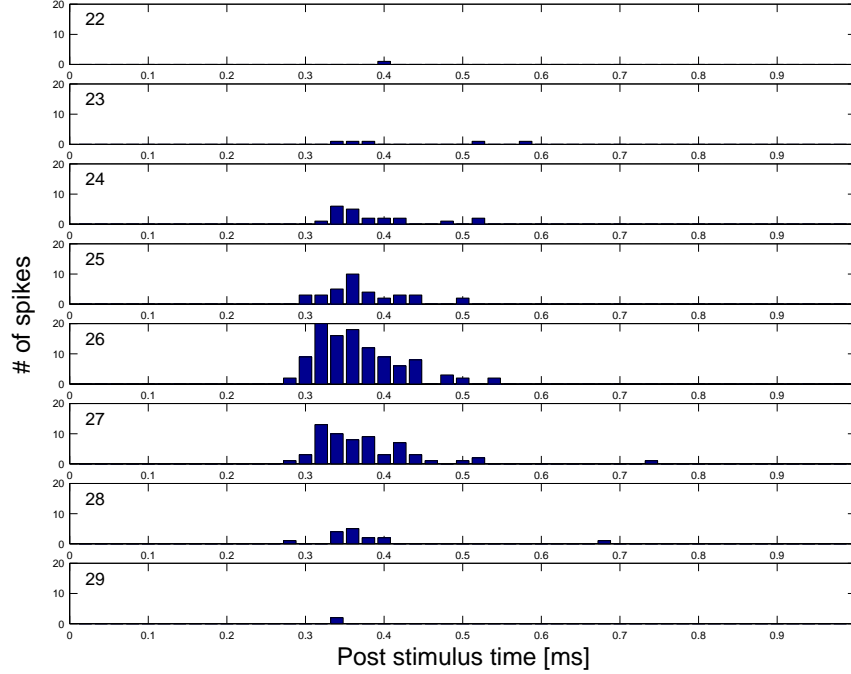


Figure 8: The PST histogram of the nodal initiation sites at the electrode-to-fiber distance of 4 mm. The PST histogram was generated from the spike times of $V_m(36, t)$'s in response to 500 identical stimulus pulses in which the spikes were initiated at the nodes from the 22th to the 29th.

in response to 500 identical stimulus pulses. The nodal initiation sites are shown in the 23th-28th in each inset. The temporal variation of spikes looks within approximately 200 μs . We note that the total number of spikes at each node in Figure 7 corresponds to the histogram of spikes initiated at each node in Figure 6 (a). We also note that the sum of the PST histograms of each node at the same time instance is identical to those of the all-nodes PST histograms shown in Figure 5 (a).

Figure 8 shows the PST histogram of the nodal initiation sites at the electrode-to-fiber distance of 4 mm. The spike times were recorded at the 36th node in response to 500 identical stimulus pulses. The node numbers initiated are shown in the 22th-29th in each inset. The temporal variation of spikes looks approximately 300 μs . Figure 9 shows the PST histogram of the spikes initiated at each node at the electrode-to-fiber of 7 mm. The spike times were recorded at the 36th node in response to 500 identical stimulus

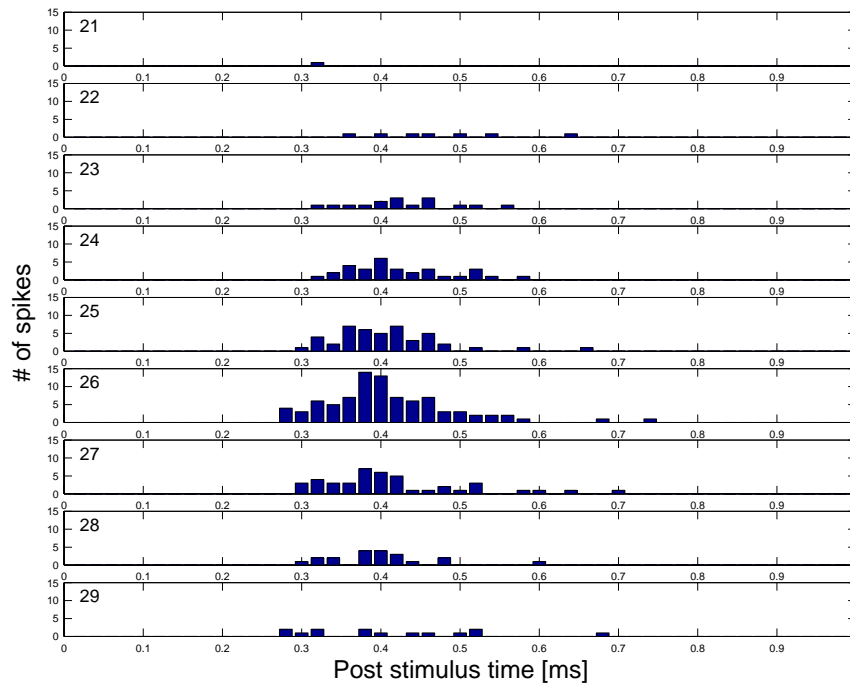


Figure 9: The PST histogram of the nodal initiation sites at the electrode-to-fiber distance of 7 mm. The PST histogram was generated from the spike times of $V_m(36, t)$'s in response to 500 identical stimulus pulses in which the spikes were initiated at the nodes from the 21th to the 29th.

pulses. The node numbers initiated are shown in the 21th-29th in each inset. The temporal variation of spikes looks approximately 400 μs at each node. It is shown in the PSTHs of each node that the temporal variation tends to be larger as the electrode-to-fiber increases. It is implied from Figures 6 through 9 that a large jitter can be generated by not only “spatial influence” but also “temporal influence”.

3.4 Discussion

In the present QPR, we have investigated the effects of the electrode-to-fiber distance on the temporal responses of spike occurrences, using the revised nerve fiber model incorporated with the advanced computational algorithm. We have shown that as the electrode-to-fiber distance increases, the jitter of spikes tends to increase, and these phenomena may be explained by interacting “spatial influence” and “temporal influence”, i.e., “spatio-temporal influence”. However, we note that the auditory nerve fiber model used here was assumed to be a straight shape and a unrealistic electrode-to-fiber distance, unlike histology in cochlea. Incorporating the detail knowledge of cochlear histology into our model, i.e., an auditory nerve fiber possessing curvatures, would produce a larger jitter due mainly to “spatial influence” even at a realistic electrode-to-fiber distance within approximately 2 mm . Therefore, it will be necessary to continue to make efforts to match the data in computational models to those recorded in experiments (Miller et al., 1999), particularly, with regard to auditory nerve fiber configurations as well as refractory properties (Miller et al., 2001a; Miller et al., 2001b). These modeling endeavors may significantly advance our understanding of information transfer in the electrically stimulated auditory nerve as well as accelerate the design of better auditory prostheses.

4 Plans for the next quarter

In the eighth quarter, we plan to do the following:

- In the eighth quarter we plan to continue work with Michigan thin film electrode, our investigations of adaptation as well as comparisons between model and single-fiber data. We plan to meet with our consultant team in August 2001.
- We will present two oral presentations and one poster at the Asilomar cochlear implant meeting. Dr Rubinstein is co-chair of this meeting

and Dr Abbas is on the steering committee.

5 Appendix: Presentations and publications

- A manuscript has been accepted for publication in the IEEE Transactions on Biomedical Engineering for the October, 2001 issue entitled “Analysis of Monophasic and Biphasic Electrical Stimulation of Nerve” by Rubinstein, Miller, Mino & Abbas.

6 Appendix: Numerical calculations

The transmembrane potential $V_m(x, t)$ is expressed in terms of space x and time t as:

$$\begin{aligned} -h^2 \frac{\partial}{\partial x} \left(\frac{1}{R_a(x)} \frac{\partial V_m(x, t)}{\partial x} \right) \\ + C_m(x) \frac{\partial V_m(x, t)}{\partial t} + \frac{V_m(x, t)}{R_m(x)} + I_{ion}(x, t) \end{aligned} \quad (1)$$

$$= h^2 \frac{\partial}{\partial x} \left(\frac{1}{R_a(x)} \frac{\partial V_e(x, t)}{\partial x} \right)$$

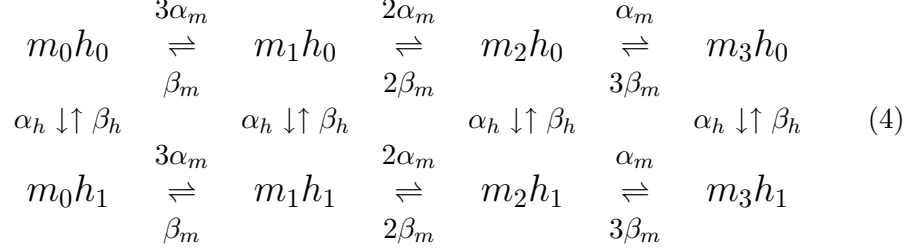
where h denotes an infinitesimal space of x , the extracellular potential $V_e(x, t)$ is represented as:

$$V_e(x, t) = \frac{\rho}{4\pi z_d} I_{app}(t) \quad (2)$$

where ρ_e , z_d , and $I_{app}(t)$ denote extracellular resistivity, the distance between the electrode and the fiber at x , and the stimulus current applied, respectively, and where $I_{ion}(x, t)$ stands for the sum of the sodium and potassium channel currents at 50 stochastic active nodes, $I_{Na}(t, x)$ and $I_K(t, x)$ generated according to Markov jumping processes:

$$I_{Na}(t, x) = \gamma_{Na} N_{m_3h_1}(t, x) (V_m(t, x) - E_{Na}) \quad (3)$$

where $N_{m_3h_1}(t, x)$ denotes the number of sodium channels staying in the state m_3h_1 at space x and time t :



where the kinetic parameters are expressed by

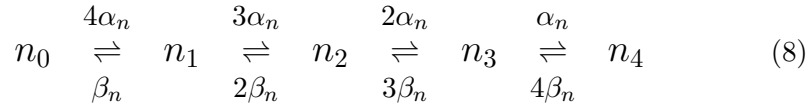
$$\begin{aligned}
 \alpha_m &= \frac{1.872(V_m - 25.41)}{1 - e^{(25.41 - V_m)/6.06}} \\
 \beta_m &= \frac{3.973(21.001 - V_m)}{1 - e^{(V_m - 21.001)/9.41}}
 \end{aligned} \quad (5)$$

$$\begin{aligned}
 \alpha_h &= \frac{-0.549(27.74 + V_m)}{1 - e^{(V_m + 27.74)/9.06}} \\
 \beta_h &= \frac{22.57}{1 + e^{(56.0 - V_m)/12.5}}
 \end{aligned} \quad (6)$$

where V_m has units of mV , and

$$I_K(t, x) = \gamma_K N_{n_4}(t, x)(V_m(t, x) - E_K) \quad (7)$$

where $N_{n_4}(t, x)$ denotes the number of potassium channels staying in the state n_4 at space x and time t :



where the kinetic parameters are expressed by

$$\begin{aligned}
 \alpha_n &= \frac{0.129(V_m - 35)}{1 - e^{(35 - V_m)/10}} \\
 \beta_n &= \frac{0.3236(35 - V_m)}{1 - e^{(V_m - 35)/10}}
 \end{aligned} \quad (9)$$

where V_m has units of mV .

In order to perform numerical calculations in digital computers, the discretized version of the transmembrane potentials, $V_m[k, t]$, is derived as functions of space k and time t :

$$\begin{aligned}
& - \left(\frac{V_m^{[k+1]}[t] - V_m^{[k]}[t]}{R_a^{[k+1,k]}} - \frac{V_m^{[k]}[t] - V_m^{[k-1]}[t]}{R_a^{[k,k-1]}} \right) \\
& \quad + C_m^{[k]} \frac{V_m^{[k]}[t + \Delta t] - V_m^{[k]}[t]}{\Delta t} + \frac{V_m^{[k]}[t]}{R_m^{[k]}} + I_{ion}^{[k]}[t] \\
& \quad = \frac{V_e^{[k+1]}[t] - V_e^{[k]}[t]}{R_a^{[k+1,k]}} - \frac{V_e^{[k]}[t] - V_e^{[k-1]}[t]}{R_a^{[k,k-1]}}
\end{aligned} \tag{10}$$

where

$$I_{ion}^{[k]}[t] = \begin{cases} \gamma_{Na} N_{Na}^{[k]}[t] (V_m^{[k]}[t] - E_{Na}) \\ \quad + \gamma_K N_K^{[k]}[t] (V_m^{[k]}[t] - E_K) & (\text{at node}) \\ 0 & (\text{otherwise}) \end{cases} \tag{11}$$

where $N_{Na}^{[k]}[t]$ and $N_K^{[k]}[t]$ stand for the number of channels being open at space k and time t for sodium and potassium channels, respectively, and

$$V_e^{[k]}[t] = \frac{\rho}{4\pi z_d} I_{app}[t] \tag{12}$$

To numerically solve the diffusive partial differential equation described above, the Crank-Nicholson method was utilized. This integration method is based on the average of explicit forward Euler and implicit backward Euler methods in which they are sort of trapezoidal rules. The Crank-Nicholson method is applied to $V_m^{[k]}[t]$ terms in the discretized PDE as follows:

$$\begin{aligned}
& C_m^{[k]} \frac{V_m^{[k]}[t + \Delta t] - V_m^{[k]}[t]}{\Delta t} \\
& = \frac{1}{2} \left\{ \frac{V_m^{[k+1]}[t + \Delta t] - V_m^{[k]}[t + \Delta t]}{R_a^{[k+1,k]}} - \frac{V_m^{[k]}[t + \Delta t] - V_m^{[k-1]}[t + \Delta t]}{R_a^{[k,k-1]}} \right. \\
& \quad \left. + \frac{V_m^{[k+1]}[t] - V_m^{[k]}[t]}{R_a^{[k+1,k]}} - \frac{V_m^{[k]}[t] - V_m^{[k-1]}[t]}{R_a^{[k,k-1]}} \right\} \\
& \quad + \frac{V_e^{[k+1]}[t] - V_e^{[k]}[t]}{R_a^{[k+1,k]}} - \frac{V_e^{[k]}[t] - V_e^{[k-1]}[t]}{R_a^{[k,k-1]}} - I_{ion}^{[k]}[t]
\end{aligned} \tag{13}$$

A simple manipulation of (13) gives an alternative expression:

$$\begin{aligned}
& \frac{V_m^{[k+1]}[t + \Delta t]}{R_a^{[k+1,k]}} - \left(\frac{1}{R_m^{[k]}} + \frac{1}{R_a^{[k+1,k]}} + \frac{1}{R_a^{[k,k-1]}} + \frac{2C_m^{[k]}}{\Delta t} \right) V_m^{[k]}[t + \Delta t] + \frac{V_m^{[k-1]}[t + \Delta t]}{R_a^{[k,k-1]}} \\
&= -\frac{V_m^{[k+1]}[t]}{R_a^{[k+1,k]}} + \left(\frac{1}{R_m^{[k]}} + \frac{1}{R_a^{[k+1,k]}} + \frac{1}{R_a^{[k,k-1]}} - \frac{2C_m^{[k]}}{\Delta t} \right) V_m^{[k]}[t] - \frac{V_m^{[k-1]}[t]}{R_a^{[k,k-1]}} \\
&\quad + 2 \left\{ -\frac{V_e^{[k+1]}[t]}{R_a^{[k+1,k]}} + \left(\frac{1}{R_a^{[k+1,k]}} + \frac{1}{R_a^{[k,k-1]}} \right) V_e^{[k]}[t] - \frac{V_e^{[k-1]}[t]}{R_a^{[k,k-1]}} + I_{ion}^{[k]}[t] \right\}
\end{aligned} \tag{14}$$

It follows from (14) that $V_m^{[k]}[t + \Delta t]$ can be determined at each time step by solving the set of K equations whose coefficients exist at only tridiagonal slices in the coefficient matrix:

$$\begin{bmatrix} b_1 & c_1 & 0 & \cdots & & & \\ a_2 & b_2 & c_2 & \cdots & & & \\ & & & \cdots & & & \\ & & & \cdots & a_{K-1} & b_{K-1} & c_{K-1} \\ & & & \cdots & 0 & a_K & b_K \end{bmatrix} \begin{bmatrix} V_m^{[1]}[t + \Delta t] \\ V_m^{[2]}[t + \Delta t] \\ \vdots \\ V_m^{[K-1]}[t + \Delta t] \\ V_m^{[K]}[t + \Delta t] \end{bmatrix} = \begin{bmatrix} RHS^{[1]}[t] \\ RHS^{[2]}[t] \\ \vdots \\ RHS^{[K-1]}[t] \\ RHS^{[K]}[t] \end{bmatrix} \tag{15}$$

where $a_1 = 0$ and $c_K = 0$, and where $RHS^{[k]}[t]$'s denote the right hand side of (14) for $k = 1, 2, \dots, K$ at time t .

References

- [1] Colombo, J., and Parkins, C.W. (1987) A model of electrical excitation of the mammalian auditory-nerve neuron. *Hear. Res.* 31, 287-312.
- [2] Finley, C.C., Wilson, B.S., White, M.W. (1990) Models of neural responsiveness to electrical stimulation in *Cochlear Implants: Models of the electrically stimulated ear* edited by J. M. Miller, F. A. Spelman, 55-96.
- [3] Frankenhauser, B., and Huxley, A.F. (1964) The action potential in the myelinated nerve fiber of *Xenopus Laevis* as computed on the basis of voltage clamped data. *J. Physiol.(Lond.)* 171, 302-315.
- [4] Hodgkin, A. L., and Huxley, A. F. (1952) A quantitative description of membrane current and its application to conduction and excitation in nerve. *J. Physiol.(Lond.)* 117, 500-544.

- [5] Matsuoka, A.J., Rubinstein, J.T., Abbas, P.J., Miller, C.A. (2001) The effects of interpulse interval on stochastic properties of electrical stimulation: models and measurements. *IEEE Trans. on Biomed. Eng.* 48, 416-424.
- [6] McNeal, D. R. (1976) Analysis of a model for excitation of myelinated nerve. *IEEE Trans. on Biomed. Eng.* 23, 329-337.
- [7] Miller, C. A., Abbas, P. J., Robinson, B. K., Rubinstein, J. T., Matsuoka, A. J. (1999) Electrically evoked single-fiber action potentials from cat: responses to monopolar, monophasic stimulation. *Hear. Res.* 130, 197-218.
- [8] Miller, C.A., Abbas, P.J., Rubinstein, J.T., Robinson B.K. (2001a) Fifth Quarterly Progress Report, N01-DC-9-2107 “The Neurophysiological Effects of Simulated Auditory Prosthesis Stimulation”.
- [9] Miller, C.A., Abbas, P.J, Robinson, B.K.(2001b) Response properties of the refractory auditory nerve fiber. *J. Assoc. Oto. Res.*, in press.
- [10] Mino, H., Rubinstein, J.T., Miller, C.A., Abbas, P.J. (2000) Fourth Quarterly Progress Report, N01-DC-9-2106 “Effects of remaining hair cells on cochlear implant function”.
- [11] Press, W.H., Teukolsky, S.A., Vetterling, W.T., Flannery, B.P. (1993) *Numerical Recipes in C : The Art of Scientific Computing*. New York, Cambridge University Press, 847-851.
- [12] Rubinstein, J.T. (1995) Threshold fluctuations in an N sodium channel model of the node of Ranvier. *Biophys. J.* 68, 779-785.
- [13] Verveen, A.A. (1961) *Fluctuation in Excitability*. Amsterdam: Drukkerij, Holland N.V.